Thermal Performance of a Pair of Synthetic Jets Equipped in Microchannel

J. Mohammadpour, G. E. Lau, S. Cheng, A. Lee

Abstract—Numerical study was conducted using two synthetic jet actuators attached underneath a micro-channel. By fixing the oscillating frequency and diaphragm amplitude, the effects on the heat transfer within the micro-channel were investigated with two synthetic jets being in-phase and 180° out-of-phase at different orifice spacing. There was a significant benefit identified with two jets being 180° out-of-phase with each other at the orifice spacing of 2 mm. By having this configuration, there was a distinct pattern of vortex forming which disrupts the main channel flow as well as promoting thermal mixing at high velocity within the channel. Therefore, this configuration achieved higher cooling performance compared to the other cases studied in terms of the reduction in the maximum temperature and cooling uniformity in the silicon wafer.

Keywords—Synthetic jets, microchannel, electronic cooling, computational fluid dynamics.

I. Introduction

THE developments and innovations of modern microprocessors have leaned towards miniaturisation and becoming rapidly powerful with the addition of new features, which leads to demand for better and more efficient thermal management. It was reported that the heat fluxes that will be generated from future microprocessors would exceed 1 MW/m^2 [1]. As the heat dissipation level from these state-of-the-art chips is rising at an exponential rate, if the cooling technology implemented is inadequate to bring down their maximum operating temperature well below 85 ℃, the chip performance will be compromised [2].

An active cooling system, known explicitly as synthetic jet actuators, is a promising cooling technology to decrease the heat flux levels of microprocessors. The synthetic jet actuators function by having fluid flowing in a micro-channel, which is directly in contact with the heated surface but simultaneously having synthetic jets impinging in the micro-channel to disrupt the thermal boundary layer and promotes better flow mixing around the heated area. A synthetic jet is produced by the time-periodic, alternating suction and discharging of fluid through a small and narrow orifice in a fluid-filled cavity [3].

Unlike conventional impinging jet, a synthetic jet is generated solely by the working fluid in the flow system. Hence, the jet is able to produce fluid flow with finite momentum without any mass addition to the flow system.

J. Mohammadpour and S. Cheng are with Macquarie University, NSW 2109, Australia (e-mail: javad.mohammadpour@mq.edu.au, shaokoon.cheng@mq.edu.au)
G.E. Lau is with Xiamen University Malaysia, 43900 Sepang, Selangor, Malaysia (e-mail: gharek.lau@xmu.edu.my)
A. Lee is with Macquarie University, NSW 2109, Australia (corresponding author, e-mail: ann.lee@mq.edu.au)

This operating condition is also known as a zero-net-mass flow which is a method that provides an efficient way to direct fluid flow across the heat source [4]. The application of synthetic jet in thermal management has emerged as a promising cooling approach [4].

Several studies have been conducted on synthetic jets based on pulsating jet actuators impinging on submerged surfaces in quiescent fluid media. In the early stage of synthetic jet development, [5] implemented a 1.6 mm diameter single synthetic jet to demonstrate that power dissipation was at least 2.5 times higher than natural convection for direct normal impingement cooling of a 49-elements multichip. Kercher et al. [6] found that the cooling performance of the micro synthetic jet coolers was higher compared to the commercial fan cooling system. Gillespie et al. [7] demonstrated the local heat transfer enhancement with synthetic jet actuators using particle image velocimetry (PIV) and validated the findings performed by previous research work performed using computational models. By using air as the cooling medium, [8] studied the enhancement of heat transfer in micro-channels using synthetic jet interacting with cross-flow fluid. They established that the introduction of the synthetic jet in a micro-channel could potentially create significant temperature reduction in the silicon wafer.

In most studies, the fluid flow is assumed laminar due to the low frequency prescribed for the oscillating membrane of the micro-scale jet actuator. Timchenko et al. [9] maintained the Reynolds number for air and fluid flow, and demonstrated that the rate of heat transfer is 55 times higher when water is used instead of air as the synthetic jet. Timchenko et al. [9] also revealed in their numerical study that the utilisation of air in microchannels has only about 37% higher over steady flow in terms of heat transfer enhancement.

Several studies have been conducted to investigate the design of the jet orifice and cavity. Utturkar et al. [10] investigated the effects of cavity aspect ratio and placement of diaphragm in quiescent and crossflow on the sensitivity of the synthetic jets. They simulated four different jet cavity designs while fixing the Reynolds number of the boundary layer at $Re_\delta = 1200$. According to their findings, changes in the cavity design had minimum effect on the jet exit flow, and there were about less than 7% differences implied on the jet exit velocity ratio between the cavity configurations. Watson et al. [11] carried out an experimental study on the number and geometry of the orifices of the synthetic jet, and their results showed that rectangular-shaped orifice has a higher tendency to form turbulent ring compared to the circular orifice.

As the development of synthetic jet progressed, [12]

World Academy of Science, Engineering and Technology
International Journal of Mechanical and Mechatronics Engineering
Vol:15, No:2, 2021

investigated the effect of having a neighbouring synthetic jet to the overall flow structure in an experiment. The study showed that the dual jet configuration in which the main jet grows in the presence of an adjacent synthetic jet caused vigorous vortical fluid motion that enhanced the flow mixing as well as a decrease in the peak value of velocity compared to a single jet configuration. Subsequently, [13] examined the effects of different actuators operating frequencies and demonstrated that they affect the size and number of the vortices formed at the upstream and downstream of the orifice in the microchannel. The results further show that higher flow velocity can be attained in the channel with higher oscillating frequency. In other research papers, Lee et al. [14], [15] studied the effect of actuator operating frequency on heat transfer in a microchannel at a fixed Reynolds number, and they demonstrated that the ideal actuator oscillating frequency was at 560 Hz and a higher reduction in silicon wafer temperature can be attained with the 180° out-of-phase jet configuration. It was further determined that the effect of actuation phases became insignificant when the operating frequency of the actuators exceeds 1120 Hz.

By simulating the numerical model of double synthetic jet actuators with separate cavities, [14] and [15] have also performed three-dimensional studies to understand the effects of flow structures caused by the in-phase and 180° out-of-phase jet configuration and when water is used as the coolant. The results from the above study showed that continuous flow mixing in the micro-channel likely created by the distinct presence of vortices was associated with the 180° out-of-phase configuration. The above studies concluded that more significant reduction in the silicon wafer maximum temperature could be achieved when the synthetic jets operate with the 180° out-of-phase configuration and the effects of spacing between the synthetic jets should be investigated to optimize the process.

In this study, computational modelling of two synthetic jet actuators attached to the channel bed and in series will be investigated. The objective of this paper is to examine how actuation phases and orifice spacings of the synthetic jet actuators affect the flow structure and heat transfer enhancement in a micro-channel. Studies were performed with the jets being in-phase and 180° out-of-phase for different orifice spacings.

II. MATHEMATICAL MODEL

The governing equations for the micro-channel flow, transformed into the two-dimensional body-fitted curvilinear coordinate system $\left(\xi^l \equiv (\varepsilon, \gamma)\right)$, are given as:

Continuity:

$$\frac{\partial \rho_l}{\partial \tau} + \frac{1}{\sqrt{g}}\left[\frac{\partial}{\partial \xi^l}\left(\rho_l\left(U^{\xi^l} - U_g^{\xi^l}\right)\right)\right] = 0 \tag{1}$$

Momentum:

$$\frac{\partial(\rho_l U_i)}{\partial \tau} + \frac{1}{\sqrt{g}}\left[\frac{\partial}{\partial \xi^l}\left(\rho_l\left(U^{\xi^l} - U_g^{\xi^l}\right)U_i\right)\right] = -\frac{1}{\sqrt{g}}\frac{\partial}{\partial \xi^l}(\beta_{il}p) +$$
$$\frac{1}{\sqrt{g}}\frac{\partial}{\partial \xi^l}\left(\mu_l\sqrt{g}g^{lm}\frac{\partial U_i}{\partial \xi^m}\right) + \frac{1}{\sqrt{g}}\frac{\partial}{\partial \xi^l}\left(\mu_l\frac{\beta_{kl}}{\sqrt{g}}\frac{\partial}{\partial \xi^m}(\beta_{lm}U_k)\right) \tag{2}$$

Enthalpy:

$$\frac{\partial(\rho_l h_l)}{\partial \tau} + \frac{1}{\sqrt{g}}\left[\frac{\partial}{\partial \xi^l}\left(\rho_l\left(U^{\xi^l} - U_g^{\xi^l}\right)h_l\right)\right] = \frac{1}{\sqrt{g}}\frac{\partial}{\partial \xi^l}\left(\frac{\xi_l}{Pr}\sqrt{g}g^{lm}\frac{\partial h_l}{\partial \xi^m}\right) \tag{3}$$

Solid Temperature:

$$\frac{\partial(\rho_s T_s)}{\partial \tau} = \frac{1}{\sqrt{g}}\frac{\partial}{\partial \xi^l}\left(\lambda_s\sqrt{g}g^{lm}\frac{\partial T_s}{\partial \xi^m}\right) \tag{4}$$

where ρ_l, μ_l and Pr are the density, dynamic viscosity and Prandtl number of the fluid and ρ_s and λ_s are the density and thermal conductivity of the solid. U_g^l are the instantaneous grid velocities in x and y directions at a fixed point (ε, γ) in the computational domain. These are:

$$U_g^1 = \left(\frac{\partial x}{\partial t}\right)_{\varepsilon, \gamma} \qquad U_g^2 = \left(\frac{\partial y}{\partial t}\right)_{\varepsilon, \gamma} \tag{5}$$

Moving mesh methodology [16] is adopted in this work. The mesh point at any point of the cavity of the synthetic jet generator is denoted as P,

$$U_g^l(P) = U_{g,mambrane}^l(P)(1 - f(d)) \tag{6}$$

where $f(d) = 0$ for $d = d_{min}$ and $f(d) = 1$ for $d = D$. The weighting function $f(d)$ may take any suitable form. For simplicity, a linear weighting function is used: $(d - d_{min})/(D - d_{min})$. The membrane velocity $U_{g,mambrane}^l(P)$ in (6) can be evaluated from analytical function. At new time instant, the nodal point locations of the mesh within the cavity of the synthetic jet generator can be determined using:

$$x^{n+1} = x^n + U_g^1(P)\Delta t$$
$$y^{n+1} = y^n + U_g^2(P)\Delta t \tag{7}$$

III. NUMERICAL SCHEME

The governing equations are discretised by the finite volume method (FVM) on a structured collocated grid arrangement. For the advection terms, the hybrid-differencing scheme, which switches between the first-order upwind differencing and second-order central differencing based on the local Peclet number, is adopted. Second-order central differencing scheme is applied for the diffusion terms and pressure gradients. The SIMPLE pressure correction algorithm

World Academy of Science, Engineering and Technology
International Journal of Mechanical and Mechatronics Engineering
Vol:15, No:2, 2021

is utilized to link the collocated velocity and pressure fields. The unsteady flow converges within the time-step upon the activation of the actuator. The algebraic forms of the governing equations are solved using the strongly implicit procedure (SIP). A fully implicit iterative procedure is adopted to obtain the unsteady solution of the fluid flow. Within each time step, convergence was ascertained when the mass residual falls below 10^{-5}.

At all stationary walls, the velocity of the fluid was set to the non-slip condition. By considering the energy balance at the boundary interfacing the liquid and sold regions, the wall temperature can be evaluated via:

$$\lambda_l \left(\frac{\partial T_l}{\partial n} \right)_i = \lambda_s \left(\frac{\partial T_s}{\partial n} \right)_i \tag{8}$$

where n refers to the outward drawn normal and the subscript i indicates an interface. For outlet and open boundaries, Neumann boundary condition is applied for the velocity components. Temperature is specified when the fluid enters the domain while Neumann boundary condition is imposed when the fluid exits the domain. The gradient of the pressure correction in the normal direction is taken to be zero at the solid boundaries. The pressure is updated by utilizing the momentum equation in the normal direction at the solid boundaries while appropriate pressure levels are prescribed at the outlet and open boundaries. For symmetry boundary, Neumann boundary condition is applied for all velocity components and temperature except for the velocity normal to the boundary which is required to be set to zero.

The numerical method and moving mesh algorithm utilized in this work have been validated in Lee et al. [13]-[16] by comparison with experimental data with all details of the grid movement methodology presented.

IV. PROBLEM DESCRIPTION

The schematic diagram of the two-dimensional computational domain using double synthetic jets in cross flow is depicted in Fig. 1. The numerical model consists of two synthetic jet actuators located underneath the micro-channel. Water flows through the open boundaries on the left to enter the channel and then leaves the computational domain through the open boundaries on the right, as shown with the dotted line in Fig. 1.

Dimensions on each part of the geometry are given in Table I. A range of orifice spacings was implemented in this project. The distances between two orifices carried out were, a = 1 mm, 2 mm and 3 mm. Structured mesh was applied to the model where the grid independence test was performed following the same approach as [14], [15]. A denser mesh was implemented at the boundary areas and orifice sections. The total mesh point is this model is 2414568. 1.5 times of the total mesh refinement was conducted and the fluid flow and heat transfer were found to be insignificant.

TABLE I
DIMENSION OF THE MODEL

Parts	Symbol	Dimension (mm)
Orifice Diameter	D_o	0.05
Orifice Height	h_o	0.1
Cavity Height	H	0.5
Diaphragm Length	L_d	1.9625
Opening Length	L_b	1
Channel Length	L	4
Channel Height	h_c	0.2
Silicon Height	h_s	0.5
Boundaries spacing	t_s	0.025

The inlet and outlet of the computational domain are treated as openings since fluid could enter or leave the region of interest through these boundaries at various times in the cycle. Chamber sizes were substantiated in front of and behind the micro-channel because fluid comes from the large pressured header, which may have many channels in parallel order as indicated in Opening in Fig. 1. The pressure difference between the two openings at the ends of the channel is kept constant at 750 Pa while the temperature is kept constant at 293 K. We have deemed the specification of a constant pressure difference as being more realistic; in any case, the "tuning" of the requisite pressure difference would have been computationally very expensive. A time-step of 1/100 of the period of oscillation of the membrane was employed.
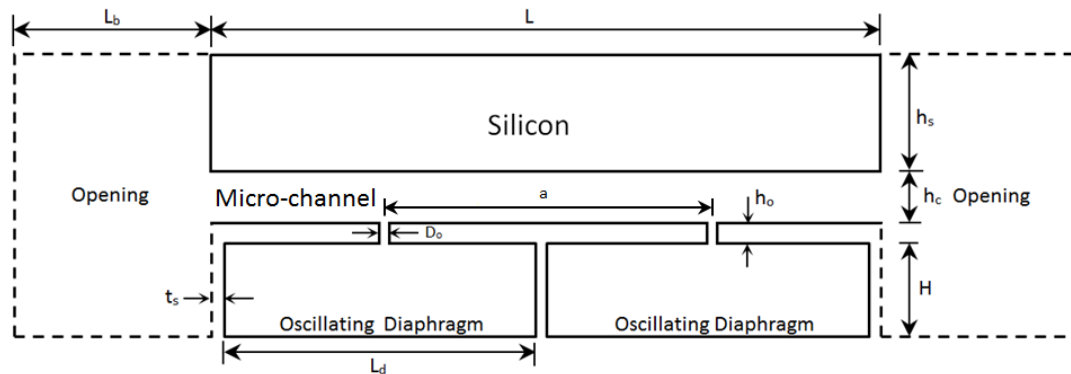

Fig. 1 Schematic diagram of double synthetic jet actuators attached to a micro-channel

World Academy of Science, Engineering and Technology
International Journal of Mechanical and Mechatronics Engineering
Vol:15, No:2, 2021

The instantaneous displacement of the membrane Y_m was taken to be

$$Y_m = A\left(1 - \left(\frac{x}{D_d/2}\right)^2\right)\sin\left(2\pi f t\right)$$

(9)

where A is the centerline amplitude, and f is the frequency of oscillation. The membrane oscillation frequency and amplitude were carried out at frequency f = 560 Hz and amplitude A = 40 μm.

V. RESULT AND DISCUSSION

The transient calculations conducted to investigate the effect of phasing and spacings on synthetic jet actuator arrays were initiated from the steady-state condition. Fig. 2 illustrates the temperature contour at orifice spacing of 2 mm in the xy-plane at the middle of the z-plane for both silicon wafer and fluid flowing in the channel. The top surface of the silicon wafer had 1 MW/m^2 of heat flux applied on it that acted as the heat source. As convective heat transfer took place across the channel, it was observed that the thermal boundary layer began to develop along the upper wall of the channel inlet which grew thicker as it travelled further down the channel outlet. By referring to the figure, the right side of the silicon wafer was found to be the hottest region. This was mainly due to the cooling of the left side of the wafer as cooler fluid flowed from the channel inlet and while the thermal boundary layer at the channel upstream started to develop. The maximum temperature in the silicon wafer was found to be similar and approximately 366 K even with having different orifice spacings jet configurations of 1 mm and 3 mm.
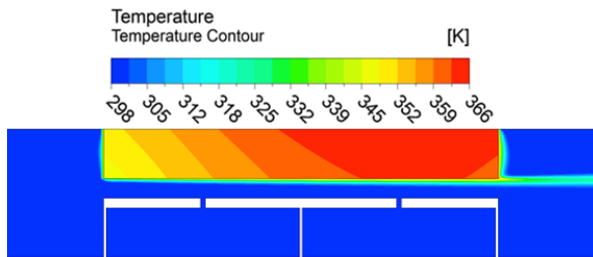

Fig. 2 Temperature contours (xy-plane) at steady state with orifice spacing of 2 mm

A. In-Phase Configuration

By fixing the actuator operating frequency at 560 Hz and the oscillating amplitude at 40 μm, the flow structures in the micro-channel were investigated for the in-phase case for orifice spacings of 1 mm, 2 mm and 3 mm. Transient calculations were performed for 40 cycles and were initiated from the acquired steady-state condition channel flow without activating the jet actuators.
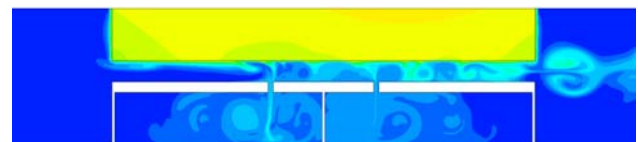
The instantaneous temperature contours at different instants during the 10th cycle generated on the xy-plane at the middle of the z-plane when the orifices were spaced 1 mm apart are shown in Fig. 3. Fig. 3 (a) shows that when both jets are ejecting upwards at maximum velocity, at the left orifice, cold fluid impinged the thermal boundary layer along the upper wall of the channel and caused thermal mixing between the hot and cold fluid from the downstream of the left jet towards the channel outlet. During the maximum suction phase at time t* = 10.5, as shown in Fig. 3 (b), hot fluid in the channel was drawn into both the left and right cavities. However, since a higher amount of cold fluid was flowing at the upstream of the left jet throughout the whole cycle, cold fluid was found ingested into the left cavity.

The instantaneous temperature contours at different instants during the 10th cycle for the in-phase jet configuration on the xy-plane at the mid-z-plane are shown in Fig. 4. At time t* = 10, there was a small amount of cold fluid near the downstream of the left jet that has interacted with the thermal boundary layer. As time passed (t* = 10.5, Fig. 4 (b)), the cold fluid swirled downwards due to the vortical motion. When compared to the previous in-phase case (Fig. 3, 1 mm orifice spacing), the cooling effect in the current case was not uniformly distributed across the entire silicon wafer where the temperature at the right side of the wafer was clearly higher. The above observation is likely caused by the fact that cold fluid entered from the left channel as well as from the left cavity which helped to reduce the temperature at the left side of the silicon wafer at a higher rate.
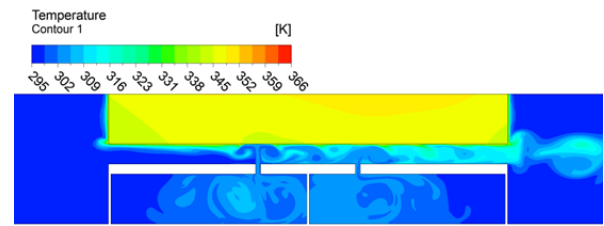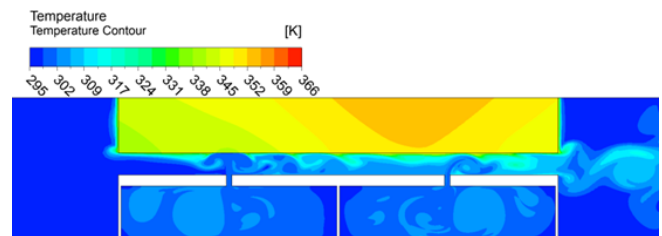

(a)

(b)

Fig. 3 Instantaneous temperature contours (xy-plane) at different instant of the 10th cycle of the in-phase oscillating case with 1 mm orifice spacing: (a) t* = 10 and (b) t* = 10.5

(a)

World Academy of Science, Engineering and Technology
International Journal of Mechanical and Mechatronics Engineering
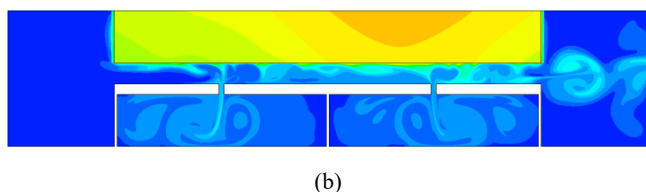Vol:15, No:2, 2021

(b)

Fig. 4 Instantaneous temperature contours (xy-plane) at different instant of the 10th cycle of the in-phase oscillating case with 2 mm orifice spacing: (a) t* = 10 and (b) t* = 10.5

The instantaneous temperature contours at different instants during the 10th cycle for the in-phase jet configuration with orifice spacing of 3 mm based on the xy-plane at the middle of the z-plane are shown in Fig. 5. Results show that the silicon wafer was not cooled down uniformly as the right side of the wafer was hotter than the left side of the wafer at all time instances. Lower temperature at the left side of the wafer was likely caused by the fact that cold fluid from the cavity was impinging the top channel wall which disrupted the thermal boundary layer during the ejection phase (see Fig. 5 (a)). Furthermore, during the maximum suction phase shown in Fig. 5 (b), due to the thermal mixing occurring around the left impingement region, the heated fluid was drawn into the left cavity and hence ingesting an amount of cold fluid from the left opening boundary that cooled down the wafer around the channel inlet.
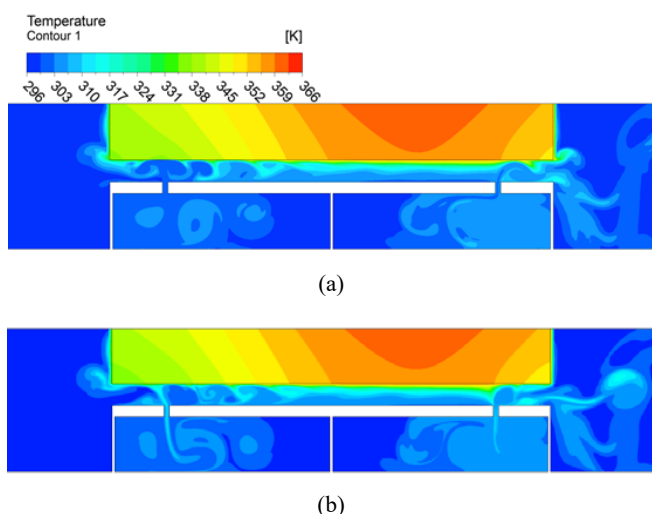

(a)

(b)

Fig. 5 Instantaneous temperature contours (xy-plane) at different instant of the 10th cycle of the in-phase oscillating case with 3 mm orifice spacing: (a) t* = 10 and (b) t* = 10.5

B. 180° Out-of-Phase Configuration

The instantaneous temperature contours at different instants during the 10th cycle for the 180° out-of-phase jet configuration with orifice spacing of 1 mm generated on the xy-plane at the mid-z-plane are shown in Fig. 6. At the instance when maximum ejection occurred at the left jet and maximum suction occurred at the right jet as depicted in Fig. 6 (a), it was shown that the cold fluid impinged from the left cavity was drawn into right cavity. The temperature in the left cavity was found to be lower than the right cavity for the

whole cycle since the cold fluid from the channel inlet was drawn into the left cavity during the suction phase for the left actuator while most of the higher temperature mixed-flow resulted from the thermal boundary layer disruption was drawn into the right cavity during the ejection phase. Furthermore, most of the mixing that occurred between the cold and hot fluid were observed around the second half of the channel. This was because there was only minimal thermal mixing between the cold fluid in the channel and the heated surface as the left orifice was far apart from the upstream of the channel. When compared to the temperature contours for the in-phase jet configuration in Fig. 3, the thermal boundary layer along the upper wall at the upstream of the left jet experienced minimum disruption, as shown in Fig. 6. The above enabled continuous thermal mixing to take place in the channel, which resulted in the cooler second half of the silicon wafer compared to the first half. In addition, when compared with the in-phase case (Fig. 3), the area of hot region in the silicon wafer for the 180° out-of-phase case was also more extensive.
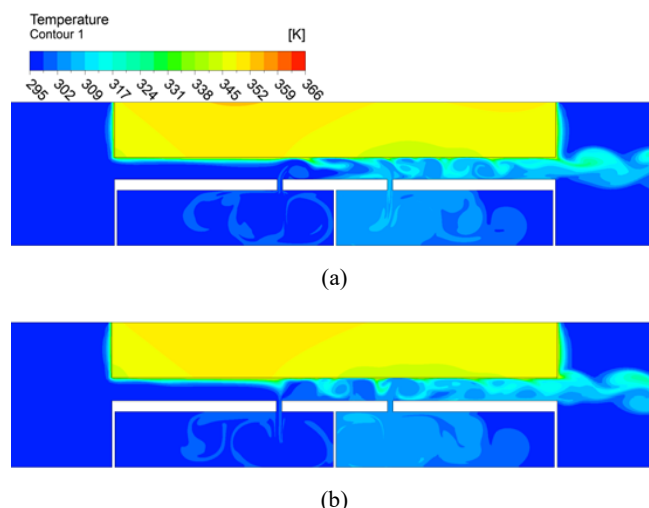

(a)

(b)

Fig. 6 Instantaneous temperature contours (xy-plane) at different instant of the 10th cycle of the out-of-phase oscillating case with 1 mm orifice spacing: (a) t* = 10 and (b) t* = 10.5

The instantaneous temperature contours at different instance during the 10th cycle for the 180° out-of-phase jet configuration with orifice spacing of 3 mm based on the xy-plane at the mid-z-plane are shown in Fig. 7. The results show that the temperature in the left cavity was significantly lower than the right cavity throughout the whole cycle. This could be explained with the out-of-phase jet arrangement at time t* = 10 in Fig. 7 (a), as maximum ejection occurred at the left jet, cold fluid was gushing out from the left cavity to disrupt the thermal boundary layer near the downstream of the left jet to cause thermal mixing from there onwards. At the same time, due to the maximum suction occurring at the right jet, it was observed that hot fluid from the thermal mixing was drawn into the right cavity. The cold fluid in the right cavity brought down the temperature of fluid coming into the channel subsequently.

World Academy of Science, Engineering and Technology
International Journal of Mechanical and Mechatronics Engineering
Vol:15, No:2, 2021

When the left actuator has undergone maximum suction at time $t^* = 10.5$ in Fig. 7 (b), a small amount of hot fluid was drawn into the left cavity due to the disruption of the thermal boundary layer during the previous time steps. However, as maximum ejection occurred at the right actuator, fluid from the cavity then spurted out to cause more thermal mixing within the channel. By comparing the temperature contours between the in-phase and out-of-phase cases for orifice with a spacing of 2 mm, it can be observed that the hot region in the wafer (Fig. 7) was smaller and hence suggested that the out-of-phase case has produced a more effective and uniform cooling effect. Furthermore, in comparison to the out-of-phase jet configuration with orifice spacing of 1 mm discussed previously, the thermal boundary layer along the upstream of the upper channel wall, in this case, was disrupted due to the continuous ejection and suction motion of the left jet. Hence, the hotter region found on the left side of the silicon wafer in the previous case was less apparent in the current case. With an orifice spacing of 2 mm, the interaction between the cold fluid and the heated surface was able to take place further downstream from the left jet. This orifice arrangement clearly alleviated the temperature difference at both sides of the silicon wafer that resulted in a more uniform cooling effect across the entire silicon wafer.
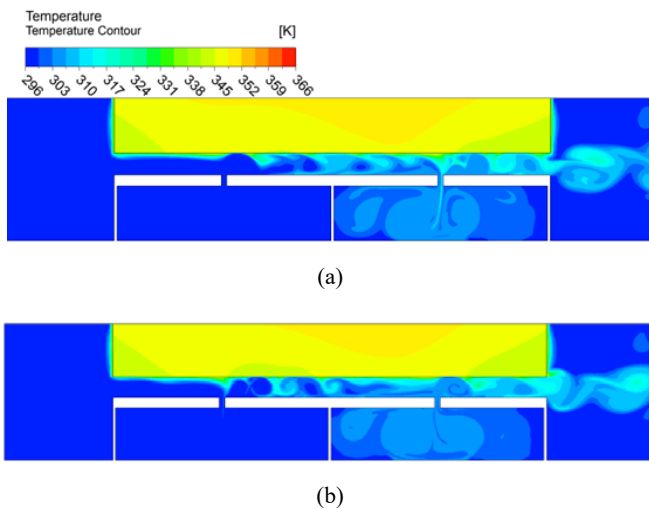

(a)

(b)

Fig. 7 Instantaneous temperature contours (xy-plane) at different instant of the 10th cycle of the out-of-phase oscillating case with 2 mm orifice spacing: (a) $t^* = 10$ and (b) $t^* = 10.5$

The instantaneous temperature contours at different instance during the 10th cycle for the 180º out-of-phase jet configuration with orifice spacing of 3 mm based on the xy-plane at the mid-z-plane are shown in Fig. 8. At time $t^* = 10$, cold fluid impinging the thermal boundary layer at the left impingement region disrupted the thermal boundary layer and resulted in thermal mixing downstream of the left jet. At the same instance, the heated fluid in the middle of the channel was seen to drawn into the right cavity.

In comparison to the in-phase case presented earlier on, the out-of-phase jet arrangement has cooled down the right part of the silicon wafer even further as the hottest region in the silicon wafer was found to be cooler than the one with the in-phase jet arrangement. The above was caused by the continuous thermal mixing between the disrupted thermal boundary layer and the cold fluid flowing in the channel, which occurred in the 180º out-of-phase case. Furthermore, by comparing the temperature contours of the current case against the other cases with different spacing configurations, it was apparent that the 3 mm orifice spacing configuration was able to cool down the left side of the silicon wafer while still leaving the right side of the wafer having a large region of hot surface.
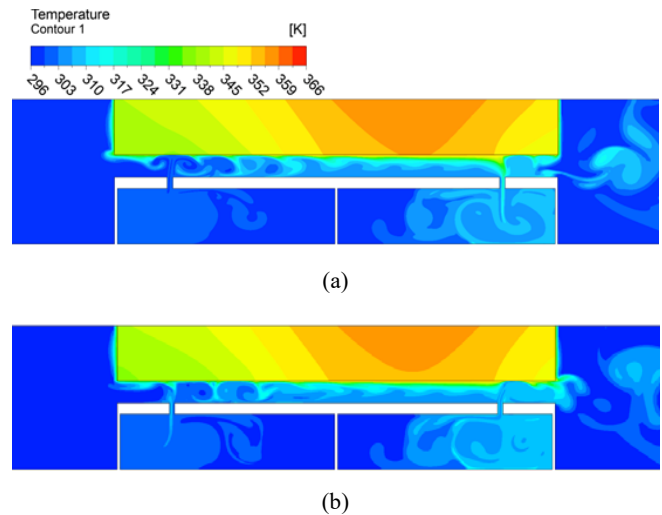

(a)

(b)

Fig. 8 Instantaneous temperature contours (xy-plane) at different instance of the 10th cycle of the out-of-phase oscillating case with 3 mm orifice spacing: (a) $t^* = 10$ and (b) $t^* = 10.5$

C. Effects of the Impingement Distance and Actuation Phase

The time history of the maximum temperature in the silicon wafer for all three spacing cases is depicted in Fig. 9 for 40 cycles of the oscillation period. It was observed that both phasing cases with orifice spacing of 1 mm exhibited the same cooling enhancement in the first six cycles. However, as time progresses, the temperature reduction was more significant for the in-phase case with orifice spacing 1 mm. Moreover, the out-of-phase case with orifice spacing of 2 mm had a smaller temperature reduction for the first eight cycles as compared to the out-of-phase case with orifice spacing of 1 mm. However, the out-of-phase jet configuration with orifice spacing of 1 mm had hotter water entraining the right cavity during the suction phase caused by the left jet impinging the thermal boundary layer, which was very close to the right orifice. In comparison to the same phasing case with orifice spacing of 2 mm, thermal mixing was allowed to take place at a greater distance, and hence the water entering the right cavity was cooler than the previous case. Therefore, this caused the fluid in the right cavity of the 1 mm spacing case to get heated up faster than the 2 mm spacing case. This explained the more significant temperature reduction for the out-of-phase case with 2 mm orifice spacing after the 8th cycle as the water impinging out from the right cavity during the ejection phase was still cooler than the 1 mm spacing case which increased

World Academy of Science, Engineering and Technology
International Journal of Mechanical and Mechatronics Engineering
Vol:15, No:2, 2021

the convective heat transfer at the downstream of the channel. It was also observed that the out-of-phase case with orifice spacing of 2 mm has eventually achieved around the same temperature reduction as the in-phase case with orifice spacing of 1 m. At the orifice spacing of 3 mm, although the out-of-phase case had greater temperature reduction as compared to the in-phase case, the cooling capability was not as effective compared to the smaller orifice spacings, i.e. 1 mm and 2 mm.
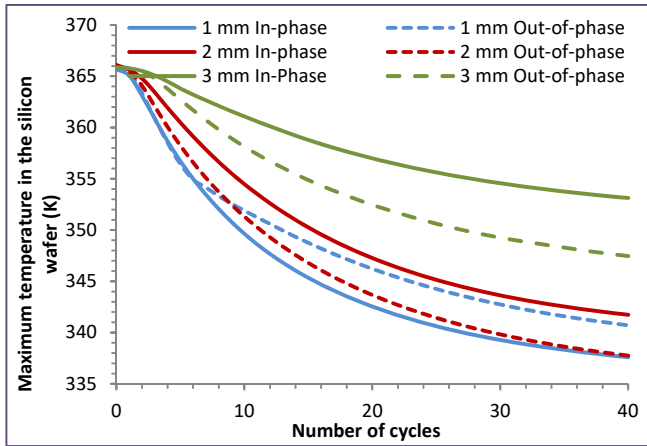

Fig. 9 Time history of the maximum temperature in the silicon wafer with different actuation phases at different orifice spacings

Table II summarises the total reduction of the maximum, average and minimum temperatures for both phasing cases with three different orifice spacings. For the in-phase jet configuration, the maximum temperatures in the silicon wafer were reduced to 337.6 K, 341.7 K and 353.1 K for the orifice spacing cases of 1 mm, 2 mm and 3 mm respectively. Subsequently, for the out-of-phase jet configuration, the maximum temperatures in the silicon wafer were reduced to 340.7 K, 337.8 K and 347.5 K for the orifice spacing cases of 1 mm, 2 mm and 3 mm respectively. Since the maximum temperature at steady state for different orifice spacing cases varied slightly, it can be concluded that the two 180° out-of-phase synthetic jets operating at orifice spacing of 2 mm achieved the highest cooling enhancement despite the small differences among the cases studied.

TABLE II
RESULT OF TEMPERATURE REDUCTION

Temperature (K)	In-phase			180° out-of-phase		
	1 mm	2 mm	3 mm	1 mm	2 mm	3 mm
Steady State	365.7	366.1	365.8	365.7	366.1	365.8
T_{max} ($t^* = 40$)	337.6	341.7	353.1	340.7	337.8	347.5
ΔT_{max}	28.1	24.4	12.7	25.0	28.3	18.3
Steady State	359.6	360.0	359.8	359.6	360.0	359.8
T_{ave} ($t^* = 40$)	335.2	336.8	345.6	336.4	334.9	340.7
ΔT_{ave}	24.4	23.2	14.2	23.2	25.1	19.1
Steady State	344.3	346.0	345.0	344.3	344.3	345.0
T_{min} ($t^* = 40$)	331.0	329.8	332.2	331.9	330.3	329.8
ΔT_{min}	13.3	16.2	12.8	12.4	14.0	15.2

VI. CONCLUSION

By fixing the operating frequency at 560 Hz and diaphragm amplitude at 40 µm for the actuator, this study demonstrates the effects of heat transfer enhancement for the in-phase and 180° out-of-phase double jets as a function of orifice spacings (1 mm, 2 mm and 3 mm).

For both phasing cases, the vortex formation is vital in unsettling the thermal boundary layer at the upper wall of the channel that leads to the mixing of the hot and cold fluid and hence dissipating heat out from the silicon wafer. However, comparing jet configurations (in-phase and out-of-phase) for orifice spacing of 1 mm, the in-phase jet configuration had a higher velocity of water flowing in the channel that increases the rate of heat dissipation. Hence, the in-phase jet configuration further reduced the maximum temperature in the silicon wafer by 3 K compared to the 180° out-of-phase jet configuration at the end of the simulation, confirming the cooling enhancement that can be potentially achieved by in-phase jet configuration with orifice spacing of 1 mm.

When the orifices were spaced at 2 mm, the maximum temperature in the silicon wafer reduced to 337.8 K for the 180° out-of-phase jet configuration which was a further drop of 4 K compared to the in-phase jet configuration. For orifices that were spaced at 3 mm, the 180° out-of-phase jet configuration achieved a further temperature reduction of 6 K compared to the in-phase jet configuration as a result of greater fluid mixing in the channel. Therefore, for orifice spacings of 2 mm and 3 mm, results from this study suggest that cooling enhancement can be potentially achieved with the 180° out-of-phase jet configuration.

The major difference in the cooling capabilities related to the cooling design configurations was likely underpinned by the distance of fluid flowing in high velocity and amount of thermal mixing in the micro-channel. As the jet impingement region was located around the middle of the channel when two orifices were spaced 1 mm apart from each other, it was found that there was a minimum disturbance on the thermal boundary layer along the upstream of the channel. This resulted in a non-uniform cooling effect on the silicon wafer and hence decreasing the cooling performance of the synthetic jets. On the other hand, there was a high velocity of fluid flowing in the middle of the channel for the case of 2 mm orifice spacing. The advantage of this jet arrangement was the continuous mixing of flow at a greater distance between the two orifices, thus improving the heat transfer enhancement to cool down the silicon wafer. However, by comparing against the cases with shorter orifice spacing, it was shown that the cooling improvements were less when two synthetic jets were generated at the orifice spacing of 3 mm. This could be explained from the fact that the left and right jet impingement regions were too far apart from each other and hence resulted in a minimum fluid mixing with low velocity in the channel that diminished the cooling capability of the jets.

In summary, the channel design configuration with double synthetic jet actuators operating at 180° out-of-phase and

World Academy of Science, Engineering and Technology
International Journal of Mechanical and Mechatronics Engineering
Vol:15, No:2, 2021

orifice spacing of 2 mm resulted in the most cooling enhancement.

REFERENCES

[1] I. Mudawar, "Assessment of high-heat-flux thermal management schemes, *IEEE Transactions on Components and Packaging Technologies"* 24 (2001) 122-141.

[2] B. Agostini, M. Fabbri, J. Park and B. Michel, "State of the art of high heat flux cooling technologies", *Heat Transfer Engineering* 28 (4) (2007) 258-281.

[3] A. Glezer and M. Amitay, Synthetic jets, *"Annual Review of Fluid Mechanics"* 34 (2002) 503-529.

[4] B.L. Smith and A. Glezer, "The formation and evolution of synthetic jets", *Phys Fluids* 10 (9) (1998) 2281-2297.

[5] M.R. Thompson, D.L. Denny, W.Z. Black, J.G. Hartly and A. Glezer, "Cooling of microelectronics devices using synthetic jet technology", *Proceedings of the 11th European Microelectronics Conference*, Venice, Italy (2007) 362-366.

[6] D.S. Kercher, J.B. Lee, O. Brand, M.G. Allen and A. Glezer, "Microjet cooling devices for thermal management of electronics", *Journal of Chemical Theory and Computation* 26 (2) (2003) 359-366.

[7] M.B. Gillspie, W.Z. Black, C. Rinehart and A. Glezer, "Local convective heat transfer from a constant heat flux flat plate cooled by synthetic air jets", *Journal of Heat Transfer* 128 (2006) 990-1000.

[8] V. Timchenko, J.A. Reizes, E. Leonardi, "An evaluation of synthetic jets for heat transfer enhancement in air-cooled micro-channels", Int. J. Num. Meth. Heat Fluid Flow 17 (2007) 263-283.

[9] V. Timchenko, J.A. Reizes, E. Leonardi, C.Y. Kwok and M. McKenzie, "Heat transfer enhancement using synthetic jet actuators in forced convection water filled microchannels", *Proceedings of the 13th International Conference on Solid State Sensors, Actuators and Microsystems*, Seoul, Korea (2005).

[10] Y. Utturkar, R. Mittal, P. Rampunggoon and L. Cattafesta, "Sensitivity of synthetic jets to the design of the jet cavity", *Proceedings of the 40th AIAA Aerospace Sciences Meeting and Exhibit*, 14-17 January 2002, Reno, Nevada, USA (2002).

[11] M. Watson, A.J. Jaworski and N.J. Wood, "A study of synthetic jets from rectangular and dual-circular orifices", *Aeronautical Journal* 107 (2003) 427-434.

[12] A. Qayoum, V. Gupta, P.K. Panigrahi and K. Muralidbar, "Influence of amplitude and frequency modulation on flow created by a synthetic jet actuator", Sensors and Actuators 162 (2010), 36-50.

[13] Lee, A., Yeoh, G.H., Timchenko, V. and Reizes, J.A., (2012) "Three Dimensional Modelling of Fluid Flow and Heat Transfer Enhancement in Microchannels Using Synthetic Jet", *International Journal of Heat and Mass Transfer*, 55, pp.198-213

[14] A. Lee, G.H. Yeoh, V. Timchenko and J.A. Reizes, "Flow structure generated by two synthetic jets in a channel: Effect of phase and frequency", *Sensors and Actuators A: Physical* 184 (2012) 98-111.

[15] A. Lee, G.H. Yeoh, V. Timchenko and J.A. Reizes, "Heat transfer enhancement in micro-channel with multiple synthetic jets", *Applied Thermal Engineering* 48 (2012) 275-288.

[16] Lee, A., Yeoh, G.H., Timchenko, V. and Reizes, J.A., (2011) "Numerical Computation and Investigation of the Characteristics of Microscale Synthetic Jets", *Modelling and Simulation in Engineering*, 2011, Retrieved Jan 16, 2012, from http://www.hindawi.com/journals/mse/2011/358940/